Solvent-induced memory effects in a model electrolyte

Sleeba Varghese [1], Benjamin Rotenberg [1,2] and Pierre Illien [1,*]

[1] *Sorbonne Université, CNRS, Physical Chemistry of Electrolytes and Interfacial Nanosystems (PHENIX), 4 place Jussieu, Paris, France*

[2] *Réseau sur le Stockage Electrochimique de l'Energie (RS2E), FR CNRS 3459, 80039 Amiens Cedex, France*

(Received 7 May 2026; accepted 23 October 2026; published 25 November 2026)

The fluctuations of ions in polar solvents remain poorly understood theoretically due to the complex coupling between ionic motion and solvent polarization. Indeed, while all-atom resolution can be achieved in numerical simulations, analytical approaches require suitable levels of coarse graining. In this work, we describe ions and solvent molecules as interacting Brownian particles and use stochastic density functional theory to derive a generalized Langevin equation for the ionic charge density, explicitly accounting for solvent-mediated memory effects. In the regime where there is a clear timescale separation between fast solvent and slow ion dynamics, we obtain simple expressions for dynamical charge structure factors, which are validated by Brownian dynamics simulations. For slow solvents, we predict an emerging two-step relaxation in ionic dynamics. These results provide a mesoscopic approach for ion-solvent dynamics and open pathways to study fluctuation-induced phenomena in electrolytes.

DOI: 10.1103/8v9p-j1w4

I. INTRODUCTION

Electrolytes play a central role in a wide range of natural and technological processes, from biological systems to energy storage devices. While their static structure and transport properties have been successfully described thanks to classical theories developed for instance by Debye, Hückel, and Onsager [1–3], capturing their dynamical properties, especially in the presence of explicit solvent fluctuations, remains a theoretical and computational challenge. Over the past decades, significant analytical progress has been made using dynamical density functional theories (DDFT) and mode-coupling theory (MCT) [4–10], which have provided insights into ionic transport, diffusion, and collective dynamics.

More recently, stochastic density functional theory (SDFT), based on the Dean-Kawasaki equation [11–13], has emerged as a powerful framework to describe fluctuations in charged systems, offering both a microscopic foundation and a systematic way to derive effective theories. SDFT has successfully reproduced a broad range of dynamical properties in electrolytes, including ionic conductivity [14–18], ionic self-diffusion [19], correlations [20–22], noise in model nanopores [23–25], and viscosity [26], while also enabling the study of fluctuation-induced phenomena such as nonequilibrium Casimir-type effects [27–32].

However, a major limitation of existing theories is their treatment of the solvent as an implicit, structureless medium. This ignores its polar nature and the nontrivial coupling between solvent and ion dynamics. For instance, in aqueous electrolytes, the dielectric nature of water controls the structure and relaxation of ions [33–36] and, in turn, the presence of ions is known to significantly affect the structure and dynamics of water even at small concentrations [37–41]. While the dynamics of polar solvents alone have been addressed within dynamical theories [42–47], the intertwined fluctuations of ions and solvent molecules, the importance of their respective timescales and of the related relaxation pathways, that have been the subject of many computational studies [48–54], remain largely unexplored in analytical approaches.

In this article, we address these challenges by deriving a generalized Langevin equation obeyed by the ionic charge density, that accounts for solvent-induced memory effects. We deduce simple yet accurate expressions for dynamic charge structure factors in the limit of a fast solvent, and confront our theoretical predictions with Brownian dynamics (BD) simulations for a model electrolyte. Beyond this fast-solvent regime, we explore the emergence of novel dynamical behaviors when the solvent relaxation time becomes comparable to or even exceeds that of the ions, that may be relevant for electrolytes in organic solvents or under supercooled conditions.

The article is organized as follows. In Sec. II, we introduce the model and the linearized SDFT equations obeyed by the ionic charge density and the solvent polarization; their derivation, and the approximations on which it relies, are detailed in Appendix A. In Sec. III, we derive a generalized Langevin equation for the ionic charge density. In Sec. IV, we analyze the limit of fast-relaxing solvents and obtain simple expressions for the dynamic charge structure factors, which are compared to Brownian dynamics simulations in Secs. V and VI. Section VII is devoted to slow-relaxing solvents, and we conclude in Sec. VIII. Analytical expressions, simulation details, and additional numerical results are gathered in Appendixes B–E.

II. STOCHASTIC DENSITY FUNCTIONAL THEORY

We consider a symmetric, binary electrolyte, in an unbounded three-dimensional volume. We denote by $\pm ze$ the charge of cations and anions (both with concentration C_I), and by $\boldsymbol{r}_i^{\pm}(t)$ their positions at time t. These ions are embedded in explicit solvent "molecules," represented as point dipoles, of

*Contact author: pierre.illien@sorbonne-universite.fr

 ©2026 American Physical Society

dipolar moment p and concentration C_S. We denote by $\boldsymbol{r}_j^S$ and $\hat{\boldsymbol{u}}_j$ the position and orientation of the jth dipole. We assume that both ions and dipoles obey overdamped Langevin dynamics. We denote by D_I and D_S the bare translational diffusion coefficients of ions and solvent molecules, respectively, and by D_S^r the rotational diffusion coefficient of solvent molecules.

We introduce the microscopic densities of cations and anions $n_\pm(\boldsymbol{r},t)=\sum_i \delta[\boldsymbol{r}-\boldsymbol{r}_i^\pm(t)]$ and that of solvent molecules $n_S(\boldsymbol{r},\hat{\boldsymbol{u}},t)=\sum_j \delta[\boldsymbol{r}-\boldsymbol{r}_j^S(t)]\delta[\hat{\boldsymbol{u}}-\hat{\boldsymbol{u}}_j(t)]$. The exact evolution equations for $n_\pm$ and n_S were derived using Itô's lemma in Ref. [55], following the procedure that leads to Dean-Kawasaki equations or stochastic density functional theory [11–13]. Details of the calculation are given in Appendix A. We linearize these equations around a constant uniform state, i.e., $n_\pm = C_I + \delta n_\pm$ and $n_S = C_S/4\pi + \delta n_S$, and we find the following equations for the ionic charge density $\rho_I = ze(\delta n_+ - \delta n_-)$:

$$\partial_t \rho_I(\boldsymbol{r},t) = D_I\nabla^2\rho_I + \varepsilon_0\kappa_I^2 D_I\nabla^2\phi + \eta_I(\boldsymbol{r},t), \tag{1}$$

where $\phi(\boldsymbol{r},t)$ is the instantaneous electrostatic potential created by all the charges in the system (ions and solvent molecules), which is determined by Poisson's equation given below, and for the solvent polarization field $\boldsymbol{P}(\boldsymbol{r},t)\equiv p\int \mathrm{d}\hat{\boldsymbol{u}}\; n_S(\boldsymbol{r},\hat{\boldsymbol{u}},t)\hat{\boldsymbol{u}} = p\int \mathrm{d}\hat{\boldsymbol{u}}\; \delta n_S(\boldsymbol{r},\hat{\boldsymbol{u}},t)\hat{\boldsymbol{u}}$:

$$\partial_t \boldsymbol{P}(\boldsymbol{r},t) = D_S\nabla^2\boldsymbol{P} - 2D_S^r\boldsymbol{P} + \frac{p^2C_S}{3k_BT}\nabla\left[D_S\nabla^2\phi - 2D_S^r\phi\right] + \boldsymbol{\eta}_S(\boldsymbol{r},t). \tag{2}$$

The range of validity of this linearization is discussed below [comment (iv)]. Here we introduced the inverse Debye screening length associated with the ions (in a medium of dielectric permittivity ε_0), $\kappa_I^2 = 2(ze)^2C_I/\varepsilon_0 k_BT$ (solvent permittivity does not appear in this definition, as it comes into play explicitly through electrostatic interactions with solvent particles), and the Gaussian noises η_I and $\boldsymbol{\eta}_S$ with zero average and correlations $\langle\eta_I(\boldsymbol{r},t)\eta_I(\boldsymbol{r}',t')\rangle = -4(ze)^2D_IC_I\delta(t-t')\nabla^2\delta(\boldsymbol{r}-\boldsymbol{r}')$ and $\langle\eta_{S,k}(\boldsymbol{r},t)\eta_{S,l}(\boldsymbol{r}',t')\rangle = (2p^2C_S/3)\delta_{kl}\delta(t-t')(-D_S\nabla^2+2D_S^r)\delta(\boldsymbol{r}-\boldsymbol{r}')$, respectively. These equations are completed with Poisson's equation, which reads as $-\nabla^2\phi = (\rho_I+\rho_S)/\varepsilon_0$, where ρ_S is the charge density associated with the solvent and ε_0 is the dielectric permittivity in vacuum. In the dipolar approximation, i.e., considering the system at distances much larger than the typical size of dipole, the solvent charge density simply reads as $\rho_S(\boldsymbol{r},t) = -\boldsymbol{\nabla}\cdot\boldsymbol{P}(\boldsymbol{r},t)$. This relation is not a definition of ρ_S: it follows from the multipole expansion of the charge distribution of each (neutral) solvent molecule, truncated at the dipolar order (see Appendix A). Taking the divergence of Eq. (2), and in Fourier space [with the convention $\tilde{\psi}(\boldsymbol{q}) = \int \mathrm{d}\boldsymbol{r}\, \mathrm{e}^{-\mathrm{i}\boldsymbol{q}\cdot\boldsymbol{r}}\psi(\boldsymbol{r})$ for any space-dependent function], we find the following linear set of equations for $\tilde{\rho}_I$ and $\tilde{\rho}_S$ [55]:

$$\partial_t\begin{pmatrix}\tilde{\rho}_I(\boldsymbol{q},t)\\ \tilde{\rho}_S(\boldsymbol{q},t)\end{pmatrix} = -\mathbf{M}\begin{pmatrix}\tilde{\rho}_I(\boldsymbol{q},t)\\ \tilde{\rho}_S(\boldsymbol{q},t)\end{pmatrix} + \begin{pmatrix}\Xi_I(\boldsymbol{q},t)\\ \Xi_S(\boldsymbol{q},t)\end{pmatrix}, \tag{3}$$

with

$$\mathbf{M} = \begin{pmatrix} D_I(q^2+\kappa_I^2) & D_I\kappa_I^2 \\ D_S\kappa_S(q)^2 & D_S(q^2+\kappa_S(q)^2)+2D_S^r\end{pmatrix}. \tag{4}$$

We introduced the wave-number-dependent screening length associated with the charge polarization of the solvent $\kappa_S(q)^2 = \frac{2p^2C_S}{3\varepsilon_0 k_BTa^2}(1+\frac{q^2a^2}{2})$ where $a\equiv(D_S/D_S^r)^{1/2}$ is the typical size of a solvent molecule, defined here through dynamical rather than structural properties. The noises Ξ_I and Ξ_S have zero average and correlations $\langle\Xi_\alpha(\boldsymbol{q},t)\Xi_\beta(\boldsymbol{q}',t')\rangle = 2q^2\varepsilon_0 k_BTD_\alpha\kappa_\alpha^2(2\pi)^3\delta(\boldsymbol{q}+\boldsymbol{q}')\delta(t-t')\delta_{\alpha\beta}$, for $\alpha\in\{I,S\}$.

Direct by-products of Eq. (3) are the charge-charge intermediate scattering functions of the model electrolyte, that are defined as $F_{\alpha\beta}(\boldsymbol{q},t)\equiv\langle\tilde{\rho}_\alpha(\boldsymbol{q},t)\tilde{\rho}_\beta(-\boldsymbol{q},0)\rangle/\sqrt{N_\alpha N_\beta}$, for $\alpha,\beta\in\{I,S\}$, and where N_I and N_S denote the total numbers of ions and solvent molecules, respectively. They typically read as $F_{\alpha\beta}(\boldsymbol{q},t) = \sum_{\nu=\pm1}\mathcal{F}_{\alpha\beta}^{(\nu)}(q)\mathrm{e}^{-\lambda_\nu|t|}$, where λ_ν are the eigenvalues of the matrix $\mathbf{M}$ and where the expressions of the weights $\mathcal{F}_{\alpha\beta}^{(\nu)}(q)$ were given in Ref. [55]. We also define the charge-charge structure factors $S_{\alpha\beta}(\boldsymbol{q}) = F_{\alpha\beta}(\boldsymbol{q},t=0)$ and dynamic structure factors $\tilde{S}_{\alpha\beta}(\boldsymbol{q},\omega) = \int_{-\infty}^{\infty}\mathrm{d}t\;\mathrm{e}^{-\mathrm{i}\omega t}F_{\alpha\beta}(\boldsymbol{q},t)$. Finally, it will be useful to consider the dynamic structure factors rescaled by their static counterpart, that we denote by $\mathcal{S}_{\alpha\beta}(\boldsymbol{q},\omega)\equiv\tilde{S}_{\alpha\beta}(\boldsymbol{q},\omega)/S_{\alpha\beta}(\boldsymbol{q})$.

The linear system of equations given in Eq. (3) is the starting point of our analysis, and several comments follow: (i) We neglected short-range, steric interactions between the ions and solvent molecules, and we considered their evolution within the dipolar approximation. Short-range repulsion is not included because it is not compatible with the linearization procedure, which assumes weak interactions, in the spirit of the Debye-Hückel approximation for electrostatic interactions [see comment (iv)]: realistic steric repulsions must diverge at small distances, and therefore cannot be treated perturbatively. Soft-core repulsive interactions, which remain finite at short distances, could be included within the same framework, but we do not expect them to change the phenomenology discussed here, and this extension is beyond the scope of this work. These two approximations (no short-range repulsion and dipolar approximation) are only expected to be valid when considering the large-scale evolution of the system, i.e., for small enough wave vector $|\boldsymbol{q}|$. In this regime, the model captures the essential physics of ion-solvent interactions. For aqueous electrolytes, it agrees with simulations that represent explicitly solvent molecules [52,55]. (ii) Without any ions, it is straightforward to show that the permittivity of the fluid of dipoles has the following Debye-type dependence on ω: $\varepsilon(\omega) = \varepsilon_0 + (\varepsilon_S-\varepsilon_0)/(1-\mathrm{i}\omega/2D_S^r)$, where $\varepsilon_S = 1+\frac{p^2C_S}{3\varepsilon_0 k_BT}$: this relates the effective static permittivity of the solvent in terms of the microscopic parameters of the model. We recently discussed the validity of such descriptions of polar solvents in the absence of ions, by systematic comparisons with BD simulations, and showed that the microscopic parameters describing the solvent could be rescaled using the Kirkwood factor (which is a measure of the local orientational correlations between neighboring dipoles) in order to account effectively for the short-range interactions between solvent particles [46]. This refinement is not necessary here but could be included in future work. (iii) The dynamic structure factors depend on both D_S and D_S^r, i.e., on both translational and rotational properties of the solvent. (iv) The linearization of the SDFT equations around a uniform state is the dynamical counterpart of the Debye-Hückel (or random

phase) approximation. It requires density fluctuations to be small compared to average densities. For the ions, this is ensured when electrostatic coupling is weak, namely, when the Bjerrum length $\ell_B = (ze)^2/(4\pi\varepsilon_0\varepsilon_S k_B T)$ is small compared to the Debye length, or equivalently when $C_I \ell_B^3 \ll 1$. For the systems simulated in this work, $C_I\ell_B^3$ ranges from 3×10^{-3} to 4×10^{-2}. Linearization does not capture strongly nonlinear effects such as ion pairing, which we account for effectively (Sec. VI). For the solvent, the corresponding coupling parameter $p^2 C_S/(3\varepsilon_0 k_B T) = \varepsilon_S - 1$ is large for waterlike solvents, and linearization amounts to a mean-field, Debye-type description of the dielectric response, which neglects local orientational correlations between dipoles; as shown in Ref. [46], this can be corrected by using effective parameters calibrated on simulations. Nonlinear couplings between density fluctuations, which would give rise to additional memory contributions of mode-coupling type [6,7], are therefore neglected in this work, and the comparison with BD simulations (Sec. VI) provides a direct test of this approximation.

III. GENERALIZED LANGEVIN DESCRIPTION

Without further approximation on the dynamics of ions and solvent molecules, one can obtain from Eq. (3) a closed equation for the ionic charge density. We solve for $\tilde\rho_S$ and reinject into the equation for $\tilde\rho_I$, which yields a generalized Langevin equation for the ionic charge density

$$\partial_t \tilde\rho_I(\boldsymbol{q},t) = -\int_{-\infty}^{t} \mathrm{d}t' \mathcal{M}(\boldsymbol{q},t-t')\tilde\rho_I(\boldsymbol{q},t') + \mathcal{X}(\boldsymbol{q},t) \quad (5)$$

with the memory kernel

$$\mathcal{M}(\boldsymbol{q},t) = 2D_I\big(q^2+\kappa_I^2\big)\delta(t) - \big(D_I\kappa_I^2\big)(D_S\kappa_S(q)^2)\mathrm{e}^{-|t|/\tau_S(q)} \quad (6)$$

and where the noise $\mathcal{X}$ is Gaussian, with zero average and correlations

$$\begin{aligned}\langle \mathcal{X}(\boldsymbol{q},t)\mathcal{X}(\boldsymbol{q}',t')\rangle &= 2q^2\varepsilon_0 k_B T D_I\kappa_I^2(2\pi)^3\delta(\boldsymbol{q}+\boldsymbol{q}') \\ &\times\left[\delta(t-t') + \frac{\tau_S(q)}{2}D_I\kappa_I^2 D_S\kappa_S(q)^2\mathrm{e}^{-|t-t'|/\tau_S(q)}\right]. \quad (7)\end{aligned}$$

We introduce the typical (q-dependent) relaxation time of the solvent: $\tau_S(q) = [D_S(q^2+\kappa_S(q)^2) + 2D_S^r]^{-1}$ [56]. The ionic counterpart to this relaxation time is obtained as the inverse of the first diagonal term of $\mathbf{M}$, and reads as $\tau_I(q) = [D_I(q^2 + \kappa_I^2)]^{-1}$. Let us specify the status of Eq. (5). Given the linear system (3), it is exact: it is obtained by solving the equation for $\tilde\rho_S$, which is linear in $\tilde\rho_I$ and Ξ_S, and by substituting the solution into the equation for $\tilde\rho_I$. This is the projection of a linear system onto one of its variables, and no mode-coupling closure is involved: the exponential part of the memory kernel simply describes the relaxation of the solvent polarization, which is driven by the ions and acts back on them with a delay. In particular, no assumption is made on the relative magnitude of the relaxation times $\tau_I(q)$ and $\tau_S(q)$, so that Eq. (5) can be used for both fast (Sec. IV) and slow (Sec. VII) solvents. Conversely, Eq. (5) inherits all the approximations underlying Eq. (3), namely, overdamped dynamics, the dipolar approximation, the neglect of short-range interactions, and the linearization of the SDFT equations.

IV. TIMESCALE SEPARATION IN FAST-RELAXING SOLVENTS

In aqueous electrolytes, a natural separation of timescales emerges because solvent and ionic motions are governed by fundamentally different physical mechanisms. Water relaxation is primarily a rotational process: individual molecules are small and can reorient through cooperative rearrangements without requiring net mass transport. As a result, polarization fluctuations of the solvent occur on picosecond timescales [57,58]. In contrast, ionic relaxation is controlled by translational diffusion, making them intrinsically much slower. Its characteristic time is typically estimated by $\varepsilon_S/(D_I\kappa_I^2)$, which is of the order of a few nanoseconds for a dilute ($\sim$0.1 M) 1:1 electrolyte in water.

We then focus on the particular limit where the solvent can be assumed to relax much faster than ions. To this end, we define two typical relaxation times: $T_I = \varepsilon_S/D_I\kappa_I^2$ and $T_S = 1/2D_S^r\varepsilon_S$, which correspond respectively to the effective relaxation times of ions and to the effective rotational time of solvent molecules, that both involve the static permittivity ε_S. Importantly, in the limit $q \to 0$ and $T_S \ll T_I$, the two eigenvalues of the matrix $\mathbf{M}$ are given by T_I^{-1} and T_S^{-1}, respectively.

Considering the limit of $T_S \ll T_I$ in the generalized Langevin equation (5) and using the general relation $\mathrm{e}^{-|u|/\epsilon} =_{\epsilon\to0} 2\epsilon\delta(u) + O(\epsilon^2)$, we find that, at leading order in the small parameter $\zeta \equiv T_S/T_I$, the ionic density obeys $\partial_t\tilde\rho_I(\boldsymbol{q},t) = -D_I[q^2+\kappa_{\mathrm{imp}}^2]\tilde\rho_I(\boldsymbol{q},t) + \tilde\eta_I(\boldsymbol{q},t)$, where $\kappa_{\mathrm{imp}} \equiv \kappa_I/\sqrt{\varepsilon_S}$ is the inverse screening length in a solvent of permittivity ε_S. This is the equation that would be obtained from the SDFT description of an electrolyte in an implicit solvent.

Going one step further in analyzing the regime $T_S/T_I \ll 1$, we now aim at finding corrections to the limit of an implicit solvent. Starting from the coupled equations for $\tilde\rho_I$ and $\tilde\rho_S$ [Eq. (3)], we deduce explicit yet lengthy expressions for the rescaled dynamical structure factors $\mathcal{S}_{\alpha\beta}$, that are written as the sum of two Lorentzian functions (see Appendix B). In the limit $T_S/T_I \ll 1$, we replace the eigenvalues $\lambda_{\pm1}$ by T_I^{-1} and T_S^{-1}, respectively, and expand the weight functions $\mathcal{F}_{\alpha\beta}^{(\nu)}(q)$ at leading order in T_S/T_I. In the $q \to 0$ limit, they take the simple form

$$\lim_{q\to0}\mathcal{S}_{\alpha\beta}(q,\omega) \simeq 2T_I\left[\frac{\mathcal{A}_{\alpha\beta}}{1+(\omega T_S)^2} + \frac{1}{1+(\omega T_I)^2}\right], \quad (8)$$

where the coefficients $\mathcal{A}_{\alpha\beta}$ are the weight of solvent contributions and read as $\mathcal{A}_{II} = \varepsilon_S(T_S/T_I)^3$, $\mathcal{A}_{IS} = -(T_S/T_I)^2$, and $\mathcal{A}_{SS} = (T_S/T_I)/\varepsilon_S$. In these three contributions, relaxation is dominated by the slow, ionic, mode of frequency T_I; but the solvent correction emerges at different order. Equation (8) is important, as it provides simple estimates for the dynamical structure factors in terms of three parameters only: the two effective relaxation times T_I and T_S, and the solvent relative permittivity ε_S. Similar but more complicated expressions are obtained for arbitrary q, and given explicitly in Appendix B.

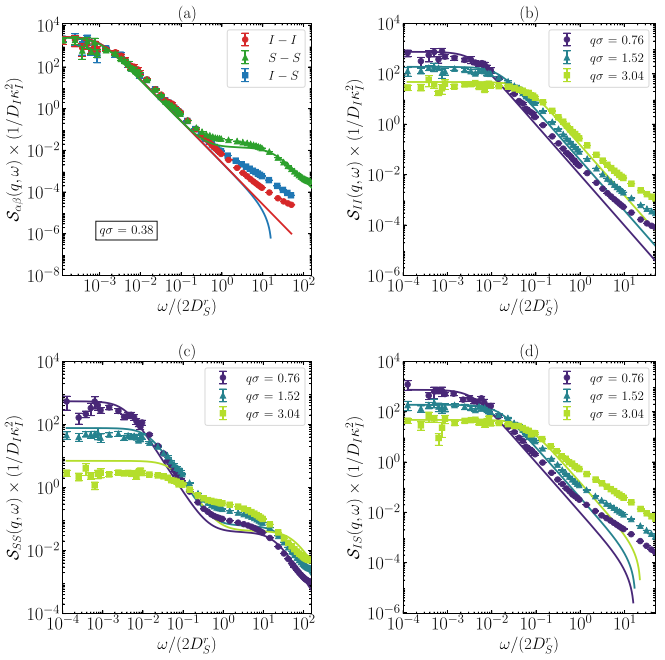


FIG. 1. Dynamic charge structure factors $\mathcal{S}_{\alpha\beta}(\boldsymbol{q}, \omega)$ measured in BD simulations (symbols) and calculated from SDFT (solid lines), (a) for the smallest wave vector accessible in the simulations and (b)–(d) for larger wave vectors (see Appendix B for analytical expressions). Error bars denote one standard error.

V. BROWNIAN DYNAMICS SIMULATIONS

In order to determine the range of validity of our approximate analytical approach, we perform BD simulations of a more realistic binary electrolyte using LAMMPS [59]. The simulated system is identical to the one studied analytically, with the difference that we add steric (Lennard-Jones–type) interactions between all particles in the system. These short-range repulsions are not included in our SDFT approach, but they are computationally necessary to counterbalance attractive interactions of electrostatic origin and prevent particle overlap.

Simulations are performed for an electrolyte with ionic concentration $C_I = 0.1\,\mathrm{M}$ and a waterlike solvent at concentration $C_S = 55\,\mathrm{M}$. The solvent dipolar strength is $p = 1.85\,\mathrm{D}$, which corresponds to a Stockmayer solvent permittivity $\varepsilon_S = 147$ according to our previous study [46]. To model transport properties, we use $D_I = 1.5\times10^{-9}\ \mathrm{m^2\,s^{-1}}$ for the ionic translational diffusion coefficient, and $D_S = 2.3\times10^{-9}\ \mathrm{m^2\,s^{-1}}$ and $D_S^r = 0.05\ \mathrm{ps^{-1}}$ ($a \simeq 2\,\text{Å}$) for the solvent translational and rotational diffusion coefficients, respectively. With these parameters, the typical relaxation times have orders of magnitude $T_I \sim 10^{-8}\,\mathrm{s}$ and $T_S \sim 10^{-14}\,\mathrm{s}$, and are therefore well separated. Further details on numerical simulations and additional results for other sets of parameters are provided in Appendixes C and D.

VI. DYNAMIC CHARGE STRUCTURE FACTORS

We first plot on Fig. 1(a) the rescaled dynamic structure factors for the smallest wave vector accessible in numerical simulations, namely, $q_{\min} = 0.38\sigma^{-1}$ ($\sigma = 3\,\text{Å}$ being the typical diameter of an ion or solvent particle in the simulations), and we use the expressions of $\mathcal{S}_{\alpha\beta}(q,\omega)$ for $q > 0$ (Appendix B) to obtain the effective values of T_I, T_S, and κ_I (we choose here to set ε_S to its previously determined value with these parameters [46], and details on the fitting procedure are provided in Appendix C 4).

First, we observe that the BD data are well described by our model over many orders of magnitude. Second, we find an effective inverse Debye length $\kappa_I^{\mathrm{eff}} = 4.2\ \mathrm{nm^{-1}}$. This is to be compared to the bare value $[2C_I(ze)^2/\varepsilon_S k_B T]^{1/2} \simeq 9.5\ \mathrm{nm^{-1}}$. This means that the effective Debye length in the simulated electrolyte is apparently larger. This can be attributed to ion pairing, which effectively reduces the concentration of free ions in simulations (see Appendix D for results on the cation-anion coordination number), and which is not accounted for in the theory. This effect is also reflected in the effective relaxation time of ions, estimated as $T_I^{\mathrm{eff}} \simeq 1.5\times10^{-7}\,\mathrm{s}$, which exceeds the bare value predicted theoretically. Finally, we find $T_S^{\mathrm{eff}} \simeq 6\times10^{-13}\,\mathrm{s}$, which is one order of magnitude higher than the bare theoretical value: this is attributed to local orientational correlations that are accounted for in the simulations, consistently with our previous results for a pure polar fluid [46].

In order to probe the validity of our approach beyond the $q \to 0$ limit, we also confront our analytical estimates to numerical simulations for higher values of q [Figs. 1(b)–1(d)]. We observe that SDFT predictions are more reliable in the low-frequency regime, while at high frequencies they only provide qualitative description of the underlying dynamics. This discrepancy cannot be attributed to the overdamped approximation since the BD simulations are themselves based on overdamped dynamics. Rather, at high frequencies, short-time dynamics is expected to be more sensitive to local steric and orientational correlations, which are present in the simulations but neglected in our linearized SDFT description. Nevertheless, Figs. 1(b)–1(d) show that for the low-frequency regime, our approach remains valid for much larger wave vectors, suggesting that slow relaxation modes are less sensitive to these microscopic details. This extends the applicability of our simplified description.

VII. TOWARD SLOW-RELAXING SOLVENTS

The results presented so far provide simple yet accurate estimates of the charge-charge correlation functions in conditions where the solvent relaxes much faster than ions. However, in ionic liquids [60,61] or under supercooled conditions [62], the timescales T_S and T_I are not expected to be well separated. We then explore the emergence of a "slow-solvent" regime, and restrict ourselves to an analytical study, as molecular simulations become computationally expensive under these conditions.

To characterize the transition between the slow- and fast-solvent regimes, we first focus on the total relaxation time of the ions, defined as $\tau_I^{\mathrm{relax}}(q) = [\int_0^\infty F_{II}(q,t)\,\mathrm{d}t]/S_{II}(q)$, and whose general expression is given in Appendix E. In the $q \to 0$ limit, it reads as $\tau_I^{\mathrm{relax}}(q=0) = T_I[1 + (\varepsilon_S - 1)\zeta]$, where $\zeta \equiv T_S/T_I$. As expected, in the limit of a fast-relaxing solvent ($\zeta \ll 1$), the ionic relaxation time is simply dominated by T_I. In the opposite limit of $\zeta \gg 1$, this relaxation time is related

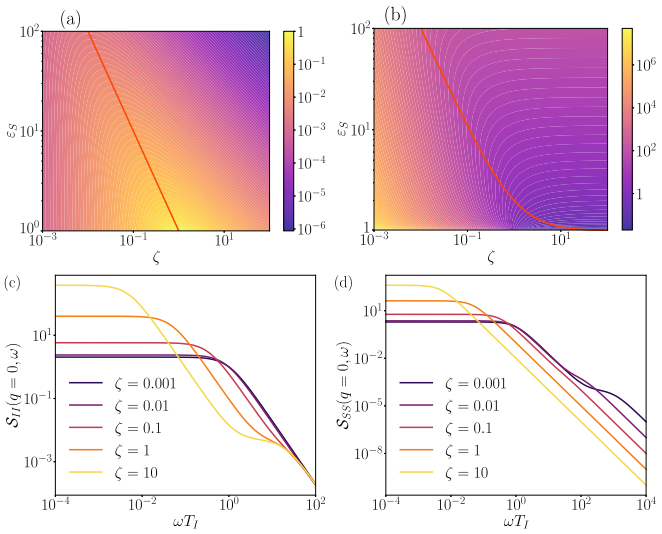


FIG. 2. Ratio of eigenvalues $\lambda_{-1}(q=0)/\lambda_1(q=0)$ (a) and weights $\mathcal{F}_{II}^{(-1)}(q=0)/\mathcal{F}_{II}^{(1)}(q=0)$ (b) as a function of $\zeta = T_S/T_I$ and ε_S. The red line indicates $\varepsilon_S = 1/\zeta$ (a), and $\varepsilon_S = 1 + 1/\zeta$ (b). Ionic (c) and solvent (d) rescaled dynamical structure factors for $\varepsilon_S = 20$ and for varying ζ. Ionic dynamics transitions from single-step relaxation ($\zeta \ll 1$) to two-step relaxation ($\zeta \gg 1$), and the opposite occurs for solvent dynamics.

to the typical solvent timescale through the relation $\tau_I^{\text{relax}}(q=0) \simeq (\varepsilon_S - 1)T_S$.

This opens the possibility for a two-step relaxation of the ion-ion dynamic charge structure factor. This can happen when the two contributions to the intermediate scattering function $\mathcal{F}_{II}^{(\pm 1)}$ occur at well-separated times but are of comparable magnitude. In order to determine the range of parameters where this may happen, we first compute the ratio between the two eigenvalues λ_{-1}/λ_1 (Appendix E). For $q = 0$, it reduces to $[1 + \zeta\varepsilon_S - \sqrt{1 + \zeta^2\varepsilon_S^2 + (2\varepsilon_S - 4)\zeta}]^2/(4\zeta)$. This expression is plotted as a function of ζ and ε_S on Fig. 2(a), and is found to reach a maximum for $\varepsilon_S\zeta = 1$. The two timescales are well separated provided that $\zeta \ll 1/\varepsilon_S$ or $\zeta \gg 1/\varepsilon_S$. Similarly, we compute the ratio between the two weights $\mathcal{F}_{II}^{(-1)}(q)/\mathcal{F}_{II}^{(1)}(q)$ (Appendix E) and plot it for $q = 0$ as a function of ζ and ε_S on Fig. 2(b). We find that the two weights can be comparable if ε_S is close enough to 1 and $\zeta \gg 1$. These observations indicate the regime where two-step relaxation of ionic fluctuations may take place. We show an example of such an unusually slow relaxation dynamics on Fig. 2(c), and the corresponding solvent-solvent contribution on Fig. 2(d).

VIII. CONCLUSION

In this article, we have studied the coupled dynamics of ions and solvent in a model electrolyte, where ions are point charges and solvent molecules are point dipoles, both undergoing overdamped translational and rotational Brownian motion. Starting from the linearized stochastic density functional theory for the ionic charge density and the solvent polarization, we derived a generalized Langevin equation for the ionic charge density, in which the coupling to the solvent results in a memory kernel and a colored noise. In the regime where the solvent relaxes much faster than the ions, we recovered the implicit-solvent description at leading order, and obtained simple expressions for the solvent contributions to the dynamic charge structure factors, which involve only the solvent permittivity and two relaxation times. The comparison with Brownian dynamics simulations showed that these expressions describe the simulated dynamics quantitatively at low frequencies, and qualitatively at high frequencies, provided that effective parameters are used to account for ion pairing and local orientational correlations between solvent molecules. Finally, in the opposite regime of slow solvents, we predicted a two-step relaxation of ionic charge fluctuations.

These findings open several avenues for future research. First, the validity of the timescale separation assumption should be systematically tested for a wider range of solvents, including those with slower relaxation dynamics. Second, the effective theory could be extended to account for spatial confinement, which is known to alter both the static and dynamic properties of electrolytes. Third, the predictions for the two-step relaxation and the slow mode could be confronted with experimental data, for example, using dielectric spectroscopy or neutron scattering techniques. Such studies would not only deepen our understanding of the fundamental physics of electrolytes but also provide valuable insights for applications in energy storage and electrochemistry.

ACKNOWLEDGMENTS

The authors thank D. Andelman for discussions. This project received funding from the European Research Council under the European Union's Horizon 2020 research and innovation program (Grant Agreement No. 863473). P.I. acknowledges financial support from Agence Nationale de la Recherche through project TraNonEq (Grant No. ANR-24-CE30-0651).

DATA AVAILABILITY

The data that support the findings of this article are openly available [63].

APPENDIX A: DERIVATION OF SDFT EQUATIONS

In this appendix, we detail the derivation of Eqs. (1) and (2) of the main text, and we state explicitly the approximations on which it relies.

1. Microscopic model

We start from the overdamped Langevin equations obeyed by the positions of the ions $\boldsymbol{r}_i^{\pm}$, the positions of the solvent molecules $\boldsymbol{r}_j^S$, and their orientations $\hat{\boldsymbol{u}}_j$ ($|\hat{\boldsymbol{u}}_j| = 1$):

$$\frac{\mathrm{d}\boldsymbol{r}_i^{\pm}}{\mathrm{d}t} = \mp\mu_I z e \nabla\phi(\boldsymbol{r}_i^{\pm}) + \sqrt{2D_I}\boldsymbol{\xi}_i^{\pm}(t), \tag{A1}$$

$$\frac{\mathrm{d}\boldsymbol{r}_j^S}{\mathrm{d}t} = -\mu_S(p\hat{\boldsymbol{u}}_j \cdot \nabla)\nabla\phi(\boldsymbol{r}_j^S) + \sqrt{2D_S}\boldsymbol{\xi}_j^S(t), \tag{A2}$$

$$\frac{\mathrm{d}\hat{\boldsymbol{u}}_j}{\mathrm{d}t} = \left\{-\mu_S^r p\left[\hat{\boldsymbol{u}}_j \times \nabla\phi(\boldsymbol{r}_j^S)\right] + \sqrt{2D_S^r}\boldsymbol{\xi}_j^{S,r}(t)\right\} \times \hat{\boldsymbol{u}}_j, \tag{A3}$$

where $\mu_I = D_I/k_\mathrm{B}T$, $\mu_S = D_S/k_\mathrm{B}T$, and $\mu_S^r = D_S^r/k_\mathrm{B}T$ are the bare mobilities associated with the bare diffusion

coefficients D_I, D_S, and D_S^r, respectively, and where the noises $\boldsymbol{\xi}_a^\alpha(t)$ are uncorrelated Gaussian white noises of zero average and unit variance, i.e., $\langle \xi_{i,n}^\alpha(t)\xi_{j,m}^\beta(t')\rangle = \delta_{\alpha\beta}\delta_{mn}\delta_{ij}\delta(t-t')$ (n, m being components of the vectors). The first term in the right-hand side of Eq. (A2) is the force exerted by the local electric field $-\nabla\phi$ on a point dipole $p\hat{\boldsymbol{u}}_j$, and the first term in the right-hand side of Eq. (A3) corresponds to the rotation induced by the electric torque $p\hat{\boldsymbol{u}}_j \times (-\nabla\phi)$.

a. Electrostatic potential. In Eqs. (A1)–(A3), $\phi(\boldsymbol{r}, t)$ is the instantaneous electrostatic potential created by all the charges in the system, i.e., by the ions and by the solvent molecules. It is the solution of Poisson's equation

$$-\nabla^2\phi(\boldsymbol{r}, t) = \frac{\rho_I(\boldsymbol{r}, t) + \rho_S(\boldsymbol{r}, t)}{\varepsilon_0}, \tag{A4}$$

where $\rho_I(\boldsymbol{r}, t) = ze[n_+(\boldsymbol{r}, t) - n_-(\boldsymbol{r}, t)]$ is the ionic charge density, with $n_\pm(\boldsymbol{r}, t) = \sum_i \delta[\boldsymbol{r} - \boldsymbol{r}_i^\pm(t)]$, and where ρ_S is the charge density carried by the solvent molecules. Each solvent molecule is neutral and is described within the dipolar approximation, i.e., its charge distribution is replaced by the lowest nonvanishing term of its multipole expansion. The charge density associated with a point dipole $p\hat{\boldsymbol{u}}_j$ located at $\boldsymbol{r}_j^S$ is $-p\,\hat{\boldsymbol{u}}_j \cdot \nabla\delta(\boldsymbol{r} - \boldsymbol{r}_j^S)$. Summing over all solvent molecules, we get

$$\begin{aligned}\rho_S(\boldsymbol{r}, t) &= -\nabla \cdot \boldsymbol{P}(\boldsymbol{r}, t),\\ \boldsymbol{P}(\boldsymbol{r}, t) &= p\sum_j \hat{\boldsymbol{u}}_j(t)\,\delta\big[\boldsymbol{r} - \boldsymbol{r}_j^S(t)\big] = p\int \mathrm{d}\hat{\boldsymbol{u}}\;\hat{\boldsymbol{u}}\,n_S(\boldsymbol{r}, \hat{\boldsymbol{u}}, t),\end{aligned} \tag{A5}$$

where $n_S(\boldsymbol{r}, \hat{\boldsymbol{u}}, t) = \sum_j \delta[\boldsymbol{r} - \boldsymbol{r}_j^S(t)]\delta[\hat{\boldsymbol{u}} - \hat{\boldsymbol{u}}_j(t)]$ is the joint position-orientation density of solvent molecules. Therefore, the relation $\rho_S = -\nabla \cdot \boldsymbol{P}$ is not a definition of ρ_S: it is a consequence of the dipolar approximation, and it is exact for point dipoles. Explicitly, the potential reads as

$$\phi(\boldsymbol{r}, t) = \frac{1}{4\pi\varepsilon_0}\int \mathrm{d}\boldsymbol{r}'\;\frac{\rho_I(\boldsymbol{r}', t) - \nabla' \cdot \boldsymbol{P}(\boldsymbol{r}', t)}{|\boldsymbol{r} - \boldsymbol{r}'|}, \tag{A6}$$

which is the continuous counterpart of Eq. (C6), used in the simulations.

b. Interpretation of the rotational noise. The noise in Eq. (A3) is multiplicative, and its interpretation must be specified. We interpret it in the Stratonovich sense, which ensures that the norm $|\hat{\boldsymbol{u}}_j| = 1$ is conserved and that, in the absence of electric torque, $\hat{\boldsymbol{u}}_j$ performs an isotropic Brownian motion on the unit sphere with rotational diffusion coefficient D_S^r. The derivation of the evolution equations for the densities relies on Itô's lemma, and must therefore start from the Itô form of Eq. (A3), which reads as

$$\begin{aligned}\mathrm{d}\hat{\boldsymbol{u}}_j = \big\{&-\mu_S^r p\big[\hat{\boldsymbol{u}}_j \times \nabla\phi\big(\boldsymbol{r}_j^S\big)\big] \times \hat{\boldsymbol{u}}_j - 2D_S^r\hat{\boldsymbol{u}}_j\big\}\mathrm{d}t\\ &+ \sqrt{2D_S^r}\,\mathrm{d}\boldsymbol{W}_j \times \hat{\boldsymbol{u}}_j,\end{aligned} \tag{A7}$$

where $\boldsymbol{W}_j$ is a Wiener process, and where the noise-induced drift $-2D_S^r\hat{\boldsymbol{u}}_j$ (the factor $2 = d - 1$ being specific to three dimensions) is the Itô correction. This choice has direct consequences on the dynamics, including at linear order: the noise-induced drift generates the rotational diffusion operator $D_S^r\boldsymbol{\mathcal{R}}^2$ in Eq. (A10) below, and it is responsible for the relaxation term $-2D_S^r\boldsymbol{P}$ in Eq. (2). In the absence of electric torque, it yields $\langle\hat{\boldsymbol{u}}_j(t)\rangle = \mathrm{e}^{-2D_S^r t}\hat{\boldsymbol{u}}_j(0)$. A naive Itô interpretation of Eq. (A3), without this drift, would conserve neither the norm of $\hat{\boldsymbol{u}}_j$ nor the isotropy of rotational diffusion. The noises in Eqs. (A1) and (A2) are additive, and their interpretation is irrelevant.

2. Dean-Kawasaki equations

The equations satisfied by $n_\pm$ are obtained following the steps of Ref. [11] (see, e.g., Refs. [14,27] for early applications to charged systems). It is convenient to write them in terms of the charge density $\rho_I = ze(n_+ - n_-)$ and total number density $\mathcal{C} = n_+ + n_-$:

$$\begin{aligned}\partial_t\rho_I =\,& D_I\nabla^2\rho_I + \mu_I(ze)^2\nabla \cdot (\mathcal{C}\nabla\phi)\\ &+ ze\nabla \cdot (\sqrt{2D_I n_+}\boldsymbol{\zeta}_+ - \sqrt{2D_I n_-}\boldsymbol{\zeta}_-),\end{aligned} \tag{A8}$$

$$\begin{aligned}\partial_t\mathcal{C} =\,& D_I\nabla^2\mathcal{C} + \mu_I\nabla \cdot (\rho_I\nabla\phi)\\ &+ \nabla \cdot (\sqrt{2D_I n_+}\boldsymbol{\zeta}_+ + \sqrt{2D_I n_-}\boldsymbol{\zeta}_-),\end{aligned} \tag{A9}$$

where $\boldsymbol{\zeta}_\pm(\boldsymbol{r}, t)$ are uncorrelated Gaussian white noises, of zero average and correlations $\langle\zeta_{\pm,n}(\boldsymbol{r}, t)\zeta_{\pm,m}(\boldsymbol{r}', t')\rangle = \delta_{nm}\delta(\boldsymbol{r} - \boldsymbol{r}')\delta(t - t')$.

The equation obeyed by the joint position-orientation density of solvent molecules $n_S(\boldsymbol{r}, \hat{\boldsymbol{u}}, t)$ is obtained similarly, by applying Itô's lemma to $\delta[\boldsymbol{r} - \boldsymbol{r}_j^S(t)]\delta[\hat{\boldsymbol{u}} - \hat{\boldsymbol{u}}_j(t)]$, with $\hat{\boldsymbol{u}}_j$ obeying Eq. (A7). Following Ref. [55], one gets

$$\begin{aligned}\partial_t n_S(\boldsymbol{r}, \hat{\boldsymbol{u}}, t) =\,& D_S\nabla_{\boldsymbol{r}}^2 n_S + D_S^r\boldsymbol{\mathcal{R}}^2 n_S + \nabla_{\boldsymbol{r}} \cdot [n_S\mu_S p(\hat{\boldsymbol{u}} \cdot \nabla)\nabla\phi]\\ &+ \boldsymbol{\mathcal{R}} \cdot \big[n_S\mu_S^r p\,\hat{\boldsymbol{u}} \times \nabla\phi\big] + \nabla_{\boldsymbol{r}} \cdot (\sqrt{2D_S n_S}\boldsymbol{\zeta}_S)\\ &+ \boldsymbol{\mathcal{R}} \cdot (\sqrt{2D_S^r n_S}\boldsymbol{\zeta}_{S,r}),\end{aligned} \tag{A10}$$

where $\boldsymbol{\mathcal{R}} = \hat{\boldsymbol{u}} \times \partial_{\hat{\boldsymbol{u}}}$ is the rotational gradient operator [64,65], and where $\boldsymbol{\zeta}_S(\boldsymbol{r}, \hat{\boldsymbol{u}}, t)$ and $\boldsymbol{\zeta}_{S,r}(\boldsymbol{r}, \hat{\boldsymbol{u}}, t)$ are uncorrelated Gaussian white noises.

3. Linearization

We now linearize Eqs. (A8)–(A10) around a constant and uniform state: $n_\pm = C_I + \delta n_\pm$ [so that $\rho_I = ze(\delta n_+ - \delta n_-)$ and $\mathcal{C} = 2C_I + c$] and $n_S = C_S/4\pi + \delta n_S$. In this state, $\phi = 0$, so that ϕ is itself of first order in the fluctuations. The range of validity of this approximation is discussed in the main text [comment (iv) of Sec. II]. At linear order, the multiplicative noises become additive, so that their interpretation no longer matters, and we get

$$\partial_t\rho_I(\boldsymbol{r}, t) = D_I\nabla^2\rho_I + \varepsilon_0\kappa_I^2 D_I\nabla^2\phi + ze\sqrt{4D_I C_I}\,\eta_I(\boldsymbol{r}, t), \tag{A11}$$

$$\partial_t c(\boldsymbol{r}, t) = D_I\nabla^2 c + \sqrt{4D_I C_I}\,\eta_c(\boldsymbol{r}, t), \tag{A12}$$

$$\begin{aligned}&\partial_t\delta n_S(\boldsymbol{r}, \hat{\boldsymbol{u}}, t)\\ &= D_S\nabla^2\delta n_S + D_S^r\boldsymbol{\mathcal{R}}^2\delta n_S + \mu_S p\frac{C_S}{4\pi}\nabla \cdot [(\hat{\boldsymbol{u}} \cdot \nabla)\nabla\phi]\\ &\quad + \mu_S^r p\frac{C_S}{4\pi}\boldsymbol{\mathcal{R}} \cdot [\hat{\boldsymbol{u}} \times \nabla\phi] + \sqrt{2D_S}\sqrt{\frac{C_S}{4\pi}}\,\eta_S(\boldsymbol{r}, \hat{\boldsymbol{u}}, t)\\ &\quad + \sqrt{2D_S^r}\sqrt{\frac{C_S}{4\pi}}\,\eta_{S,r}(\boldsymbol{r}, \hat{\boldsymbol{u}}, t),\end{aligned} \tag{A13}$$

where we used $2\mu_I(ze)^2C_I = \varepsilon_0\kappa_I^2 D_I$, by definition of the Debye screening length, and where we introduced the scalar noises $\eta_I = \boldsymbol{\nabla}\cdot(\boldsymbol{\zeta}_+ - \boldsymbol{\zeta}_-)/\sqrt{2}$, $\eta_c = \boldsymbol{\nabla}\cdot(\boldsymbol{\zeta}_+ + \boldsymbol{\zeta}_-)/\sqrt{2}$, $\eta_S = \boldsymbol{\nabla}\cdot\boldsymbol{\zeta}_S$, and $\eta_{S,r} = \boldsymbol{\mathcal{R}}\cdot\boldsymbol{\zeta}_{S,r}$. They are uncorrelated, have zero average, and correlations

$$\langle\eta_I(\boldsymbol{r},t)\eta_I(\boldsymbol{r}',t')\rangle = \langle\eta_c(\boldsymbol{r},t)\eta_c(\boldsymbol{r}',t')\rangle = -\delta(t-t')\nabla_{\boldsymbol{r}}^2\delta(\boldsymbol{r}-\boldsymbol{r}'), \quad \text{(A14)}$$

$$\langle\eta_S(\boldsymbol{r},\hat{\boldsymbol{u}},t)\eta_S(\boldsymbol{r}',\hat{\boldsymbol{u}}',t')\rangle = -\delta(t-t')\delta(\hat{\boldsymbol{u}}-\hat{\boldsymbol{u}}')\nabla_{\boldsymbol{r}}^2\delta(\boldsymbol{r}-\boldsymbol{r}'), \quad \text{(A15)}$$

$$\langle\eta_{S,r}(\boldsymbol{r},\hat{\boldsymbol{u}},t)\eta_{S,r}(\boldsymbol{r}',\hat{\boldsymbol{u}}',t')\rangle = -\delta(t-t')\delta(\boldsymbol{r}-\boldsymbol{r}')\boldsymbol{\mathcal{R}}^2\delta(\hat{\boldsymbol{u}}-\hat{\boldsymbol{u}}'). \quad \text{(A16)}$$

Equation (A12) is decoupled from the others and does not need to be considered. Equation (A11) is Eq. (1) of the main text. The evolution of the polarization $\boldsymbol{P} = p\int \mathrm{d}\hat{\boldsymbol{u}}\,\hat{\boldsymbol{u}}\,\delta n_S$ is obtained by multiplying Eq. (A13) by $p\hat{\boldsymbol{u}}$ and integrating over orientations. To this end, we use $\int \mathrm{d}\hat{\boldsymbol{u}}\,u_k u_l = (4\pi/3)\delta_{kl}$, the fact that the Cartesian components of $\hat{\boldsymbol{u}}$ are eigenfunctions of $\boldsymbol{\mathcal{R}}^2$ with eigenvalue -2 (they are $\ell = 1$ spherical harmonics), and $\int \mathrm{d}\hat{\boldsymbol{u}}\,u_k\boldsymbol{\mathcal{R}}\cdot[\hat{\boldsymbol{u}}\times\boldsymbol{\nabla}\phi] = -\int \mathrm{d}\hat{\boldsymbol{u}}\,(\hat{\boldsymbol{u}}\times\hat{\boldsymbol{e}}_k)\cdot(\hat{\boldsymbol{u}}\times\boldsymbol{\nabla}\phi) = -(8\pi/3)\partial_k\phi$, obtained by integration by parts on the unit sphere. This yields Eq. (2), together with the expression of the noise correlations given in the main text. Finally, Eqs. (1) and (2) are closed by Poisson's equation (A4) with $\rho_S = -\boldsymbol{\nabla}\cdot\boldsymbol{P}$ [Eq. (A5)]. In Fourier space, $\tilde{\phi}(\boldsymbol{q},t) = [\tilde{\rho}_I(\boldsymbol{q},t) + \tilde{\rho}_S(\boldsymbol{q},t)]/(\varepsilon_0 q^2)$, and taking the divergence of Eq. (2) leads to the closed linear system (3) for $\tilde{\rho}_I$ and $\tilde{\rho}_S$.

APPENDIX B: ANALYTICAL EXPRESSIONS OF DYNAMICAL STRUCTURE FACTORS

In this appendix, we give the general expression of the rescaled dynamic charge structure factors $\mathcal{S}_{\alpha\beta}(\boldsymbol{q},\omega)$. For the sake of conciseness, we will express them in terms of the dimensionless wave vector $Q = qa$. It is most convenient to write them as

$$\mathcal{S}_{\alpha\beta}(Q,\omega) = \sum_{\nu=\pm1}\mathcal{W}_{\alpha\beta}^{(\nu)}(Q)\frac{1}{[\omega/\lambda_\nu(Q)]^2}, \quad \text{(B1)}$$

where, in terms of the rescaled variables, the eigenvalues read as

$$T_I\lambda_{\pm1}(Q) = \frac{(Q^2+2\zeta\varepsilon_S+2)K_I^2 + 2Q^2\zeta\varepsilon_S \pm \Delta}{4K_I^2\zeta}, \quad \text{(B2)}$$

where we introduced the dimensionless Debye length $K_I = \kappa_I a$ and where we defined

$$\Delta = \sqrt{4\left(K_I^2+Q^2\right)^2\varepsilon_S^2\zeta^2 + K_I^4(Q^2+2)(Q^2-8\zeta+2) - 4K_I^2\zeta(Q^2+2)(Q-K_I)(K_I+Q)\varepsilon_S}. \quad \text{(B3)}$$

The weights $\mathcal{W}_{\alpha\beta}^{(\nu)}(Q)$ read as

$$\mathcal{W}_{II}^{(1)}(Q) = \frac{2\zeta T_I}{\Delta(Q^2+2)}\frac{\left(2\zeta\varepsilon_S\left(K_I^2+Q^2\right)\right)^2 - \left(\Delta - K_I^2(Q^2+2)\right)^2}{\Delta + K_I^2(Q^2+2) + 2\zeta\varepsilon_S\left(K_I^2+Q^2\right)}, \quad \text{(B4)}$$

$$\mathcal{W}_{II}^{(-1)}(Q) = \frac{2\zeta T_I}{\Delta(Q^2+2)}\frac{\left(\Delta + K_I^2(Q^2+2)\right)^2 - \left(2\zeta\varepsilon_S\left(K_I^2+Q^2\right)\right)^2}{K_I^2(Q^2+2) + 2\zeta\varepsilon_S\left(K_I^2+Q^2\right) - \Delta}, \quad \text{(B5)}$$

$$\mathcal{W}_{SS}^{(1)}(Q) = \frac{T_I K_I^2}{\Delta\left(K_I^2+Q^2\right)\varepsilon_S}\frac{K_I^4(Q^2+2)^2 - \left(\Delta - 2\zeta\varepsilon_S\left(K_I^2+Q^2\right)\right)^2}{\Delta + K_I^2(Q^2+2) + 2\zeta\varepsilon_S\left(K_I^2+Q^2\right)}, \quad \text{(B6)}$$

$$\mathcal{W}_{SS}^{(-1)}(Q) = \frac{T_I K_I^2}{\Delta\left(K_I^2+Q^2\right)\varepsilon_S}\frac{\left(\Delta + 2\zeta\varepsilon_S\left(K_I^2+Q^2\right)\right)^2 - K_I^4(Q^2+2)^2}{K_I^2(Q^2+2) + 2\zeta\varepsilon_S\left(K_I^2+Q^2\right) - \Delta}, \quad \text{(B7)}$$

$$\mathcal{W}_{IS}^{(1)}(Q) = \frac{4\zeta T_I K_I^2\left(\Delta - K_I^2(Q^2+2) - 2\zeta\varepsilon_S\left(K_I^2+Q^2\right)\right)}{\Delta\left(\Delta + K_I^2(Q^2+2) + 2\zeta\varepsilon_S\left(K_I^2+Q^2\right)\right)}, \quad \text{(B8)}$$

$$\mathcal{W}_{IS}^{(-1)}(Q) = \frac{4\zeta T_I K_I^2\left(\Delta + K_I^2(Q^2+2) + 2\zeta\varepsilon_S\left(K_I^2+Q^2\right)\right)}{\Delta\left(K_I^2(Q^2+2) + 2\zeta\varepsilon_S\left(K_I^2+Q^2\right) - \Delta\right)}. \quad \text{(B9)}$$

In the limit $T_S \ll T_I$, we get the approximated, q-dependent dynamic structure factors:

$$\mathcal{S}_{II}(q,\omega) \simeq 2T_I\left[\frac{8\varepsilon_S(\varepsilon_S-1)\left(q^2+\kappa_I^2/\varepsilon_S\right)}{\kappa_I^2(q^2a^2+2)^3}\left(\frac{T_S}{T_I}\right)^3\frac{1}{1+[\omega\bar{\tau}_S(q)]^2} + \frac{\kappa_I^2/\varepsilon_S}{q^2+\kappa_I^2/\varepsilon_S}\frac{1}{1+[\omega\bar{\tau}_I(q)]^2}\right], \quad \text{(B10)}$$

$$\mathcal{S}_{IS}(q,\omega) \simeq 2T_I\left[-\frac{4\varepsilon_S\left(q^2+\kappa_I^2/\varepsilon_S\right)}{\kappa_I^2(q^2a^2+2)^2}\left(\frac{T_S}{T_I}\right)^2\frac{1}{1+[\omega\bar{\tau}_S(q)]^2} + \frac{\kappa_I^2/\varepsilon_S}{q^2+\kappa_I^2/\varepsilon_S}\frac{1}{1+[\omega\bar{\tau}_I(q)]^2}\right], \quad \text{(B11)}$$

$$\mathcal{S}_{SS}(q,\omega) \simeq 2T_I\left[\frac{2\varepsilon_S\left(q^2+\kappa_I^2/\varepsilon_S\right)}{(2+q^2a^2)\left(q^2+\kappa_I^2\right)\varepsilon_S}\left(\frac{T_S}{T_I}\right)\frac{1}{1+[\omega\bar{\tau}_S(q)]^2} + \frac{\kappa_I^4(\varepsilon_S-1)}{\varepsilon_S^2\left(q^2+\kappa_I^2/\varepsilon_S\right)\left(q^2+\kappa_I^2\right)}\frac{1}{1+[\omega\bar{\tau}_I(q)]^2}\right], \quad \text{(B12)}$$

TABLE I. Details of the representative systems used in this study. In the second column, values in parentheses denote the number of ion pairs. In the fourth column, the solvent permittivity values are taken from Ref. [46].

System label	Molarity	Solvent dipole moment	Permittivity
I	0.1 M (8)	1.85 D	146.5
II	0.1 M (8)	1.665 D	64.07
III	0.4 M (30)	1.85 D	146.5

with

$$\bar{\tau}_S(q) = \frac{T_S}{1+q^2a^2/2}; \quad \bar{\tau}_I(q) = \frac{T_I}{1+\varepsilon_S q^2/\kappa_I^2}. \tag{B13}$$

Finally, in the limit $q \to 0$, they reduce to the expression given in the main text.

APPENDIX C: NUMERICAL SIMULATIONS AND DATA ANALYSIS

1. Equations of motion

In the overdamped limit, the dynamics of the ion positions $\boldsymbol{r}_i^{\pm}$ (N_I cations and N_I anions), and positions and orientations of the N_S solvent particles ($\boldsymbol{r}_j^S$ and $\hat{\boldsymbol{u}}_j$, respectively) are governed by

$$\frac{\mathrm{d}\boldsymbol{r}_i^{\pm}}{\mathrm{d}t} = -\mu_I \sum_{\substack{k=1\\k\neq i}}^{N_I+N_S} \nabla_i U^{\mathrm{rep}}_{\alpha_i\alpha_k}(|\boldsymbol{r}_k - \boldsymbol{r}_i|) \mp \mu_I(ze)\nabla\phi(\boldsymbol{r}_i^{\pm}) + \sqrt{2D_I}\boldsymbol{\xi}_i^{\pm}(t), \tag{C1}$$

$$\frac{\mathrm{d}\boldsymbol{r}_j^S}{\mathrm{d}t} = -\mu_S \sum_{\substack{k=1\\k\neq j}}^{N_I+N_S} \nabla_j U^{\mathrm{rep}}_{S\alpha_k}\left(|\boldsymbol{r}_k - \boldsymbol{r}_j^S|\right) - \mu_S(p\hat{\boldsymbol{u}}_j\cdot\nabla)\nabla\phi\left(\boldsymbol{r}_j^S\right) + \sqrt{2D_S}\boldsymbol{\xi}_j^{S,t}(t), \tag{C2}$$

$$\frac{\mathrm{d}\hat{\boldsymbol{u}}_j}{\mathrm{d}t} = \left\{-\left[\mu_S^r p\hat{\boldsymbol{u}}_j \times \nabla\phi\left(\boldsymbol{r}_j^S\right)\right] + \sqrt{2D_S^r}\boldsymbol{\xi}_j^{S,r}(t)\right\} \times \hat{\boldsymbol{u}}_j, \tag{C3}$$

where $\alpha_i \in \{+,-,S\}$ denotes the species of particle i, and where $U^{\mathrm{rep}}_{\alpha\beta}$ is a Lennard-Jones potential:

$$U^{\mathrm{rep}}_{\alpha\beta}(r) = \begin{cases} 4\epsilon_{\alpha\beta}\left[\left(\frac{\sigma_{\alpha\beta}}{r}\right)^{12} - \left(\frac{\sigma_{\alpha\beta}}{r}\right)^{6}\right] & \text{if } r \leqslant r_c, \\ 0 & \text{if } r > r_c, \end{cases} \tag{C4}$$

where r_c is a cutoff radius. The stochastic term $\boldsymbol{\xi}_a^{\alpha}(t)$ corresponds to uncorrelated Gaussian white noises of zero average and unit variance, i.e., $\langle \xi_{i,n}^{\alpha}(t)\xi_{j,m}^{\beta}(t')\rangle = \delta_{\alpha\beta}\delta_{mn}\delta_{ij}\delta(t-t')$, where n or m are components of the vectors and Greek letters refer to particle labels. Finally, $\phi(\boldsymbol{r})$ is the electrostatic potential, which is obtained by solving Poisson's equation:

$$-\nabla^2\phi(\boldsymbol{r}) = \frac{\rho(\boldsymbol{r})}{\varepsilon_0} = \frac{\rho_I(\boldsymbol{r}) + \rho_S(\boldsymbol{r})}{\varepsilon_0}, \tag{C5}$$

where ρ_I and ρ_S are the charge density associated with ions and solvent, respectively. Within the dipolar approximation, it reads as

$$\phi(\boldsymbol{r}) = \frac{1}{4\pi\varepsilon_0}\left[\sum_{\epsilon=\pm}\sum_{i=1}^{N_I}\frac{\epsilon(ze)}{\left|\boldsymbol{r}-\boldsymbol{r}_i^{\epsilon}\right|} + \sum_{j=1}^{N_S}\frac{p\hat{\boldsymbol{u}}_j\cdot\left(\boldsymbol{r}-\boldsymbol{r}_j^S\right)}{\left|\boldsymbol{r}-\boldsymbol{r}_j^S\right|^3}\right]. \tag{C6}$$

2. Simulation details

Brownian dynamics simulations consist of a numerical integration of Eqs. (C1)–(C3). To this end, we use the large scale atomic/molecular massively parallel simulator [59] (LAMMPS) package, and the BROWNIAN package [66,67]. In addition to the system described in the main text (system I), we consider two additional sets of parameters (systems II and III). All the parameters are summarized in Table I. In all cases, the temperature and solvent density are fixed at $T = 298$ K and $C_S \simeq 0.033$ Å^{-3} (55 M), respectively.

The Lennard-Jones and diffusion parameters for the ions are

$$\varepsilon_{II} = \epsilon_{++} = \epsilon_{--} = \epsilon_{+-} = 0.1 \text{ kcal mol}^{-1}, \tag{C7}$$

$$\sigma_{II} = \sigma_{++} = \sigma_{--} = \sigma_{+-} = 3.0 \text{ Å}, \tag{C8}$$

$$D_I = D_+ = D_- = 1.5\times10^{-9} \text{ m}^2 \text{ s}^{-1}. \tag{C9}$$

The Lennard-Jones interaction parameters for the Stockmayer fluid were taken from Ramirez *et al.* [68], and the related simulation parameters are summarized in Table II. The ion-solvent cross-interaction parameters are determined using the Lorentz-Berthelot mixing rule.

For all simulations, we use a cubic box of a side dimension $L = 50$ Å, with periodic boundary conditions (PBC) in all the coordinate directions. Thus, the smallest accessible wave vector, compatible with the PBC, is $2\pi/L = 0.126$ Å^{-1}, which corresponds to $q_{\min}\sigma \simeq 0.38$. Short-range steric interactions are computed using Eq. (C4), with a real space cutoff $r_c = 7.56$ Å. Short-range electrostatic interactions are computed using the definition of the electrostatic potential [Eq. (C6)], which combines contributions from ions and solvent molecules. Long-range electrostatic interactions are computed using the particle-mesh Ewald (PME) algorithm

TABLE II. Simulation parameters for the Stockmayer solvent.

Symbol	Definition	Value
σ_{SS}	LJ diameter	3.024 Å
ϵ_{SS}	LJ energy	0.4412 kcal mol^{-1}
D_S	Solvent translational diffusion coefficient	2.3×10^{-9} m^2 s^{-1}
D_S^r	Solvent rotational diffusion coefficient	0.05 ps^{-1}

TABLE III. Values of parameters used in the SDFT predictions. For the "bare" values, we use $D_S^r = 0.05$ ps^{-1} and set D_I to the long-time ionic diffusion coefficient (see Table IV for each system). Parameters marked with superscript "eff" indicate calibrated values used in computing the dynamic charge structure factors. For all cases (including system I) $a = 0.214$ nm.

System	κ_I^{bare} (nm^{-1})	$T_S^{\text{bare}}\left(=\frac{1}{2D_S^r\varepsilon_S}\right)$ (ps)	$T_I^{\text{bare}}\left(=\frac{\varepsilon_S}{D_I\kappa_I^2}\right)$ (ps)	κ_I^{eff} (nm^{-1})	T_S^{eff} (ps)	T_I^{eff} (ps)
II	9.50	0.156	1.39×10^4	2.96	0.741	1.88×10^5
III	18.4	0.0682	8.49×10^3	10.0	0.565	1.14×10^4

[69], implemented in LAMMPS, with a relative root mean square error in the per-atom force calculations below 10^{-4}.

All simulations employed a time step of 5 fs. For the systems with $C_I = 0.1$ M, trajectories of 1 μs were generated, with observables sampled every 200 fs. For the system with $C_I = 0.4$ M, simulations were run for a duration of 300 ns for four independent initial configurations, with data collected at the same sampling rate as the 0.1 M systems. All systems were initially equilibrated for a duration of 5 ns prior to data acquisition stage.

3. Dynamic charge structure factors from simulations

The partial Fourier components of the ionic charge density, and the longitudinal and transverse polarization densities, are sampled every 200 fs during the production run of the simulation, for selected wave vectors in the range $q\sigma \in [0.38, 3.42]$, satisfying $q = 2\pi m/L$ with $m \in \mathbb{N}$ to ensure compatibility with periodic boundary conditions. The dynamic structure factor is computed for each wave vector using the fast Fourier transform algorithm, applied over n blocks of the time series assumed to be statistically independent. For the system with $C_I = 0.4$ M, the results are further averaged over the four independent initial conditions, with uncertainties estimated as the standard error across the independent trajectories.

4. Fitting procedure

The calibration proceeds as follows: (i) Perform regression fitting on the simulation data of longitudinal polarization density dynamic structure factor $\mathcal{S}_{SS}(q,\omega)$, for the smallest accessible wave vector ($q_{\min}$). The fitting is carried out using the analytical expression of $\mathcal{S}_{SS}(q,\omega)$ in the $q \to 0$ limit (see main text), which yields fit values for T_S^{fit}, T_I^{fit}, and $\varepsilon_S^{\text{fit}}$. (ii) Next, we combine the $q = 0$ and $q > 0$ expressions for $\mathcal{S}_{SS}(q,\omega)$, to obtain the relation $1/\varepsilon_S^{\text{fit}} = \frac{2(q^2+\kappa_I^2/\varepsilon_S)}{(2+q^2a^2)(q^2+\kappa_I^2)}$. This expression is then used to determine κ_I^{eff}. In this step, as well as in the next, we set ε_S to the permittivity of a pure solvent. (iii) Finally, the optimal values for T_S^{eff} and T_I^{eff} are obtained from $\bar{\tau}_S(q_{\min}) = \frac{T_S^{\text{eff}}}{1+(q_{\min}a)^2/2}$ and $\bar{\tau}_I(q_{\min}) = \frac{T_I^{\text{eff}}}{1+\varepsilon_S(q_{\min}/\kappa_I^{\text{eff}})^2}$, together with the conditions $\bar{\tau}_S(q_{\min}) = T_S^{\text{fit}}$ and $\bar{\tau}_I(q_{\min}) = T_I^{\text{fit}}$.

APPENDIX D: ADDITIONAL NUMERICAL RESULTS

1. Dynamic charge structure factors: Additional results

This section compares SDFT predictions with BD results for the additional systems considered in this study. As explained in the previous section, we first apply the calibration methodology to obtain the optimal values for κ_I, T_S, and T_I. Table III summarizes the calibrated parameters, while Figs. 3–5 present comparisons between SDFT predictions and BD results for the dynamic charge structure factors. As discussed in the main text, SDFT shows excellent agreement with BD across all systems, particularly in the low-frequency regime, even at large wave vectors. Figures 4 and 5 further demonstrate a clear quantitative separation between the regimes dominated by the two relaxation modes predicted by SDFT. For $\mathcal{S}_{II}(\boldsymbol{q},\omega)$ and $\mathcal{S}_{IS}(\boldsymbol{q},\omega)$, solvent contributions are negligible, and the dynamics is dominated by the ionic relaxation mode. Whereas, for $\mathcal{S}_{SS}(\boldsymbol{q},\omega)$ in the case of fast-relaxing solvents, we can clearly see the distinct two-step relaxation, with the high frequency regime governed by the solvent relaxation and the low frequency regime controlled by the ionic relaxation.

2. Comparison of calibrated parameters

Figure 6 illustrates the variation of the calibrated parameters across the different electrolyte systems considered in this study. One key consequence of increasing solvent permittivity is the slowing down of solvent relaxation dynamics [46], which is clearly evident in Fig. 6(a). Solvent permittivity also plays a crucial role in determining the extent of ion pairing within an electrolyte. Lower permittivity leads to weaker electrostatic screening, promoting the formation of ion pairs, also known as Bjerrum pairs. Figure 6(b) shows the cation-anion coordination number for the 0.1 M systems. The nonzero coordination number within the first coordination sphere indicates the presence of ion pairing. As mentioned above, the extent of ion pairing is strongly influenced by the solvent

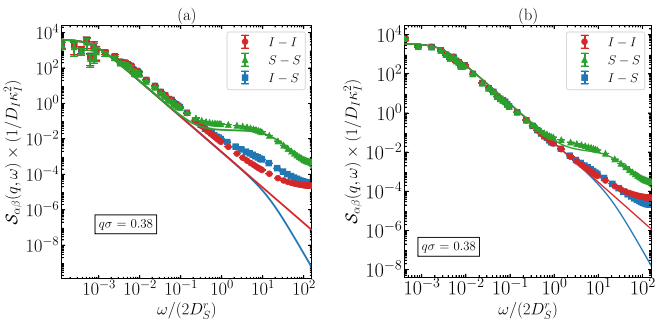


FIG. 3. Dynamic charge structure factors $\mathcal{S}_{\alpha\beta}(\boldsymbol{q},\omega)$ measured in Brownian dynamics simulations (symbols) and calculated from SDFT (solid lines), for the smallest wave vector accessible in the simulations. The SDFT estimates are obtained using the $q = 0$ expressions (see main text). The values for the fit parameters ($\varepsilon_S^{\text{fit}}$, T_S^{fit}, T_I^{fit}), for systems II (a) and III (b) are (6.26, 0.714 ps, 1.50×10^4 ps) and (76.6, 0.546 ps, 3.472×10^3 ps), respectively. The error bars denote one standard error.

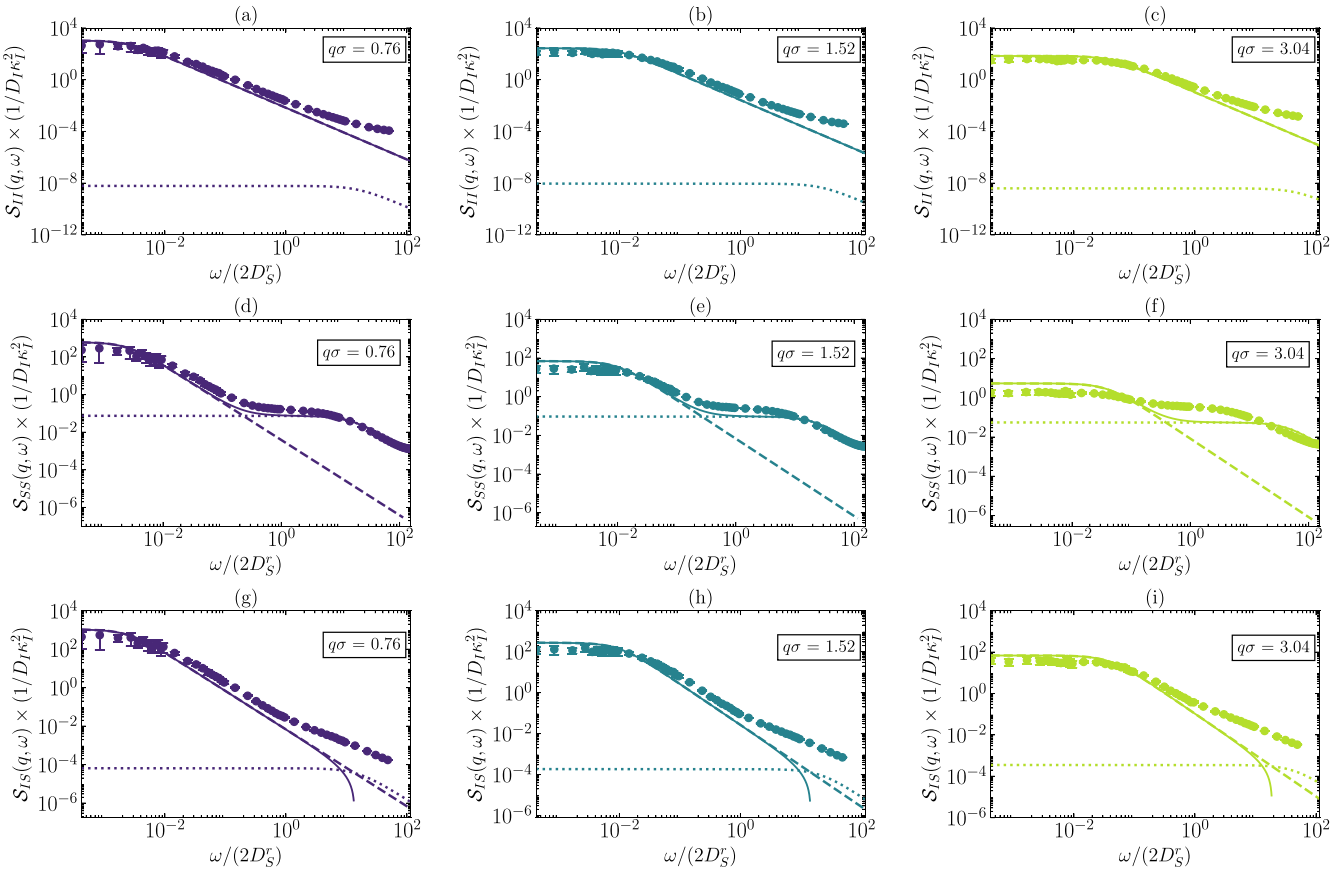


FIG. 4. Dynamic charge structure factors $\mathcal{S}_{\alpha\beta}(\boldsymbol{q}, \omega)$ at larger wave vectors for system II, calculated from Brownian dynamics simulations (symbols) and SDFT (lines). Solid lines show the full SDFT predictions based on Eqs. (B10)–(B12), while dashed lines denote contribution from their second term only. In (a)–(f) dotted lines represent the contribution from the first term of Eqs. (B10) and (B12), whereas in (g)–(i) they correspond to the opposite of the first term of Eq. (B11). The error bars denote one standard error.

permittivity, with lower permittivity solvents favoring greater ion association. This reduces the concentration of free ions available for screening, resulting in an effective ionic concentration that is lower than that of a fully dissociated electrolyte [70,71]. This behavior is reflected in the calibrated values of κ_I since $\kappa_I \propto \sqrt{C_I}$. Figure 6(c) shows the percentage reduction in κ_I relative to its nominal value, denoted by α, for the different systems. As expected, the largest reduction ($\sim$70%) occurs for the system with the lowest solvent permittivity ($\varepsilon_S = 64.07$), whereas systems with higher permittivity ($\varepsilon_S = 146.5$) exhibit more moderate reductions, with $\alpha \sim 40\%$–50%. Finally, the ionic relaxation times, shown in Fig. 6(d), indicate the fastest relaxation for the 0.4 M system, as anticipated, while the 0.1 M systems exhibit relatively similar values of T_I^{eff}.

3. Translational diffusion coefficient

In this section, we examine the effect of interactions on the transport properties of an electrolyte system. Figure 7 shows the mean square displacement (MSD) of both ion and solvent particles undergoing Brownian motion. From MSD we can obtain the particle diffusion coefficient by fitting its long-time behavior to $6Dt$. At short times, both species follow their respective bare diffusion coefficients, followed by a caging regime at intermediate times, and a long-time diffusive plateau. The corresponding long-time diffusion coefficients, extracted from the MSD and summarized in Table IV, are governed primarily by steric interactions, with electrostatic contributions remaining negligible. We further find that the presence of ions does not measurably affect the translational diffusion of the solvent, in a 0.1 M electrolyte system (Table IV). Importantly, Fig. 7(a) offers a corrected estimate for the ionic diffusion coefficient D_I used in calibrating the SDFT model, as the present SDFT framework requires the steady-state value of this parameter.

TABLE IV. Long-time diffusion coefficients calculated from the MSD. The corresponding bare values for the ion and solvent translation diffusion coefficients are $D_I = 1.5\times10^{-9}$ m^2 s^{-1} and $D_S = 2.3\times10^{-9}$ m^2 s^{-1}, respectively.

System (ε_S, C_I)	Ion diffusion coefficient (m^2 s^{-1})	Solvent diffusion coefficient (m^2 s^{-1})
Electrolyte (146.5, 0.1 M)	5.10×10^{-11}	2.96×10^{-10}
Electrolyte (64.07, 0.1 M)	3.45×10^{-11}	3.04×10^{-10}
Polar fluid (146.5)		3.12×10^{-10}
Polar fluid (64.07)		3.01×10^{-10}

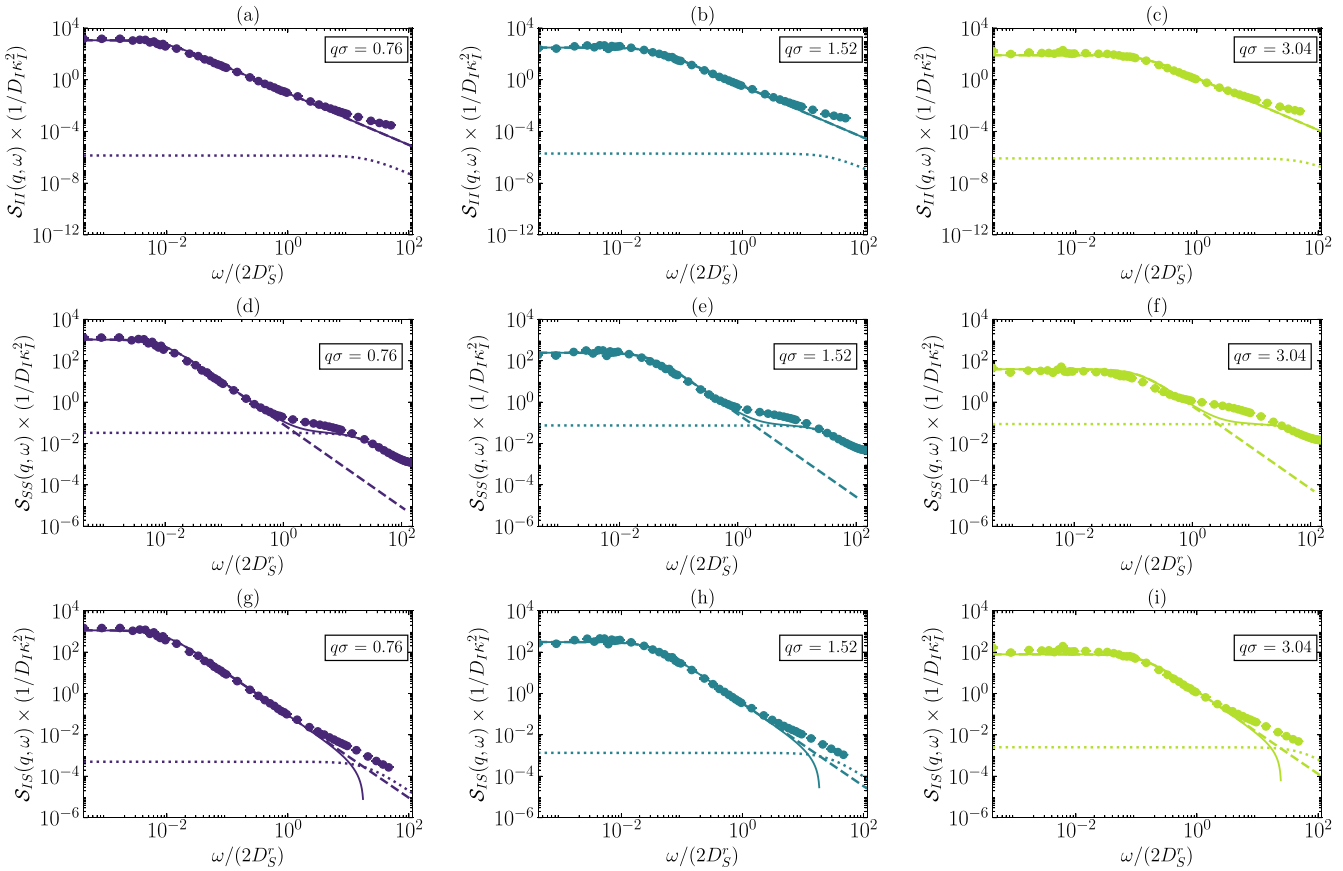


FIG. 5. Dynamic charge structure factors $\mathcal{S}_{\alpha\beta}(\boldsymbol{q}, \omega)$ at larger wave vectors for system III, calculated from Brownian dynamics simulations (symbols) and SDFT (lines). Solid lines show the full SDFT predictions based on Eqs. (B10)–(B12), while dashed lines denote contribution from their second term only. In (a)–(f) dotted lines represent the contribution from the first term of Eqs. (B10) and (B12), whereas in (g)–(i) they correspond to the opposite of the first term of Eq. (B11). The error bars denote one standard error.

APPENDIX E: BEYOND THE LIMIT OF A FAST-RELAXING SOLVENT

From the general expressions in Appendix B, we deduce the observables that are discussed in the main text.

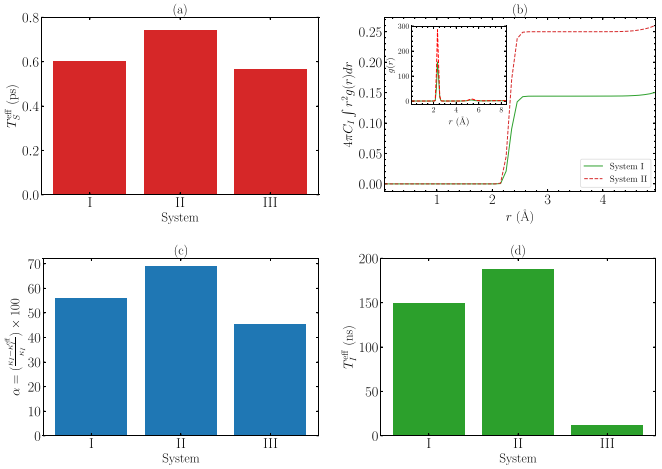


FIG. 6. (a), (c), (d) Variation of calibrated parameters across studied systems. (b) Cation-anion coordination number for the 0.1 M systems. Inset plot in (b) is the radial distribution function between cation and anion.

First, the ionic relaxation time is defined as $\tau_I^{\text{relax}}(q) = [\int_0^\infty F_{II}(q,t)\,\mathrm{d}t]/S_{II}(q)$, for any q. In dimensionless variables, we get

$$\tau_I^{\text{relax}}(Q) = \frac{K_I^2 T_I\left(Q^2 + 2\zeta\varepsilon_S - 2\zeta + 2\right)}{(Q^2+2)\left(K_I^2 + Q^2\varepsilon_S\right)}. \tag{E1}$$

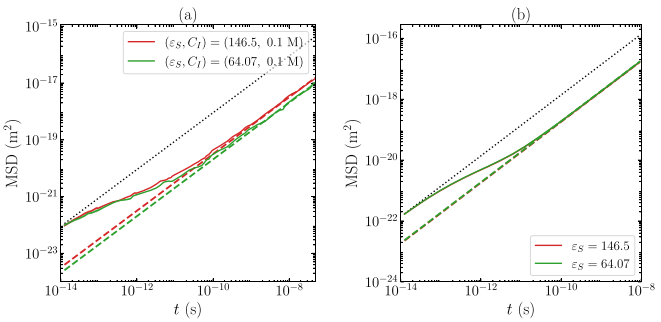


FIG. 7. Mean square displacement plots for the (a) ion and (b) solvent particles. Solid lines correspond to MSD data from BD simulations and dashed lines represent $6D_\alpha^{\text{fit}}t$, where D_α^{fit} is the long-time diffusion coefficient and $\alpha \in \{I, S\}$. The dotted line denotes the MSD plot for the noninteracting particles limit. Plots in (a) are based on electrolyte systems, while the plots in (b) are obtained from polar fluid systems.

For $Q = 0$, we retrieve the expression given in the main text. Second, the ratio between the two eigenvalues $\lambda_{\pm 1}$ reads as

$$\frac{\lambda_{-1}(Q)}{\lambda_1(Q)} = \frac{(Q^2 + 2\zeta\varepsilon_S + 2)K_I^2 + 2Q^2\zeta\varepsilon_S - \Delta}{(Q^2 + 2\zeta\varepsilon_S + 2)K_I^2 + 2Q^2\zeta\varepsilon_S + \Delta}. \tag{E2}$$

Finally, the ratio between the two weights $\mathcal{F}_{II}^{(\pm 1)}$ reads as

$$\frac{\mathcal{F}_{II}^{(-1)}(Q)}{\mathcal{F}_{II}^{(1)}(Q)} = -\frac{\left[\Delta + \left((2\varepsilon_S - 4)\zeta + Q^2 + 2\right)K_I^2 - 2Q^2\zeta\varepsilon_S\right]^2}{-16K_I^2Q^2\zeta^2\varepsilon_S^2 - 16K_I^4\zeta^2\varepsilon_S + 16K_I^2Q^2\zeta^2\varepsilon_S + 16K_I^4\zeta^2} \tag{E3}$$

which yields, in the limit $Q \to 0$,

$$\frac{\mathcal{F}_{II}^{(-1)}(0)}{\mathcal{F}_{II}^{(1)}(0)} = \frac{\left(\zeta\varepsilon_S + \sqrt{\zeta^2\varepsilon_S^2 + 2\zeta\varepsilon_S - 4\zeta + 1} - 2\zeta + 1\right)^2}{4\zeta^2(\varepsilon_S - 1)}. \tag{E4}$$

[1] H. S. Harned and B. B. Owen, *The Physical Chemistry of Electrolyte Solutions*, American Chemical Society Monograph Series (American Chemical Society, Columbus, OH, 1943).

[2] P. Résibois, *Electrolyte Theory: An Elementary Introduction to a Microscopic Approach* (Harper and Row, New York, 1968).

[3] R. A. Robinson and R. H. Stokes, *Electrolyte Solutions* (Dover, New York, 2002).

[4] T. Yamaguchi, T. Matsuoka, and S. Koda, A theoretical study on the frequency-dependent electric conductivity of electrolyte solutions, J. Chem. Phys. **127**, 234501 (2007).

[5] S. Roy, S. Yashonath, and B. Bagchi, Mode coupling theory analysis of electrolyte solutions: Time dependent diffusion, intermediate scattering function, and ion solvation dynamics, J. Chem. Phys. **142**, 124502 (2015).

[6] B. Bagchi and R. Biswas, Ionic mobility and ultrafast solvation: Control of a slow phenomenon by fast dynamics, Acc. Chem. Res. **31**, 181 (1998).

[7] A. Chandra and B. Bagchi, Ion conductance in electrolyte solutions, J. Chem. Phys. **110**, 10024 (1999).

[8] A. Chandra and B. Bagchi, Frequency dependence of ionic conductivity of electrolyte solutions, J. Chem. Phys. **112**, 1876 (2000).

[9] J.-F. Dufrêche, O. Bernard, P. Turq, A. Mukherjee, and B. Bagchi, Ionic self-diffusion in concentrated aqueous electrolyte solutions, Phys. Rev. Lett. **88**, 095902 (2002).

[10] J.-F. Dufrêche, O. Bernard, and P. Turq, Transport in electrolyte solutions: Are ions Brownian particles? J. Mol. Liq. **118**, 189 (2005).

[11] D. S. Dean, Langevin equation for the density of a system of interacting Langevin processes, J. Phys. A: Math. Gen. **29**, L613 (1996).

[12] K. Kawasaki, Stochastic model of slow dynamics in supercooled liquids and dense colloidal suspensions, Phys. A **208**, 35 (1994).

[13] P. Illien, The Dean–Kawasaki equation and stochastic density functional theory, Rep. Prog. Phys. **88**, 086601 (2025).

[14] V. Démery and D. S. Dean, The conductivity of strong electrolytes from stochastic density functional theory, J. Stat. Mech. (2016) 023106.

[15] Y. Avni, D. Andelman, and H. Orland, Conductance of concentrated electrolytes: Multivalency and the Wien effect, J. Chem. Phys. **157**, 154502 (2022).

[16] Y. Avni, R. M. Adar, D. Andelman, and H. Orland, Conductivity of concentrated electrolytes, Phys. Rev. Lett. **128**, 098002 (2022).

[17] H. Bonneau, V. Démery, and É. Raphaël, Temporal response of the conductivity of electrolytes, J. Stat. Mech. (2023) 073205.

[18] H. Bonneau, Y. Avni, D. Andelman, and H. Orland, Frequency-dependent conductivity of concentrated electrolytes: A stochastic density functional theory, J. Chem. Phys. **161**, 244501 (2024).

[19] O. Bernard, M. Jardat, B. Rotenberg, and P. Illien, On analytical theories for conductivity and self-diffusion in concentrated electrolytes, J. Chem. Phys. **159**, 164105 (2023).

[20] H. Bonneau, V. Démery, and E. Raphaël, Stationary and transient correlations in driven electrolytes, J. Stat. Mech. (2025) 033201.

[21] A. Donev, A. L. Garcia, J. P. Péraud, A. J. Nonaka, and J. B. Bell, Fluctuating hydrodynamics and Debye-Hückel-Onsager theory for electrolytes, Curr. Opin. Electrochem. **13**, 1 (2019).

[22] J. P. Péraud, A. J. Nonaka, J. B. Bell, A. Donev, and A. L. Garcia, Fluctuation-enhanced electric conductivity in electrolyte solutions, Proc. Natl. Acad. Sci. USA **114**, 10829 (2017).

[23] M. Zorkot, R. Golestanian, and D. J. Bonthuis, The power spectrum of ionic nanopore currents: The role of ion correlations, Nano Lett. **16**, 2205 (2016).

[24] M. Zorkot, R. Golestanian, and D. J. Bonthuis, Current fluctuations in nanopores: The effects of electrostatic and hydrodynamic interactions, Eur. Phys. J. Spec. Top. **225**, 1583 (2016).

[25] M. Zorkot and R. Golestanian, Current fluctuations across a nano-pore, J. Phys.: Condens. Matter **30**, 134001 (2018).

[26] P. Robin, Correlation-induced viscous dissipation in concentrated electrolytes, J. Chem. Phys. **160**, 064503 (2024).

[27] D. S. Dean and R. Podgornik, Relaxation of the thermal Casimir force between net neutral plates containing Brownian charges, Phys. Rev. E **89**, 032117 (2014).

[28] B.-S. Lu, D. S. Dean, and R. Podgornik, Out-of-equilibrium thermal Casimir effect between Brownian conducting plates, Europhys. Lett. **112**, 20001 (2015).

[29] S. Mahdisoltani and R. Golestanian, Long-range fluctuation-induced forces in driven electrolytes, Phys. Rev. Lett. **126**, 158002 (2021).

[30] S. Mahdisoltani and R. Golestanian, Transient fluctuation-induced forces in driven electrolytes after an electric field quench, New J. Phys. **23**, 073034 (2021).

[31] G. Du, D. S. Dean, B. Miao, and R. Podgornik, Correlation decoupling of Casimir interaction in an electrolyte driven by external electric fields, Phys. Rev. Lett. **133**, 238002 (2024).

[32] G. Du, D. S. Dean, B. Miao, and R. Podgornik, Repulsive thermal van der Waals interaction in multispecies asymmetric electrolytes driven by external electric fields, Phys. Rev. E **111**, 044108 (2025).

[33] J. Hubbard and L. Onsager, Dielectric dispersion and dielectric friction in electrolyte solutions. I., J. Chem. Phys. **67**, 4850 (1977).

[34] R. Buchner and G. Hefter, Interactions and dynamics in electrolyte solutions by dielectric spectroscopy, Phys. Chem. Chem. Phys. **11**, 8984 (2009).

[35] J. Yang, S. Kondrat, C. Lian, H. Liu, A. Schlaich, and C. Holm, Solvent effects on structure and screening in confined electrolytes, Phys. Rev. Lett. **131**, 118201 (2023).

[36] V. Démery, D. Toquer, and H. Berthoumieux, Effect of solvent structure on the Wien effect and ionic correlations at the nanoscale, Faraday Discuss. **266**, 361 (2026).

[37] L. Belloni, D. Borgis, and M. Levesque, Screened Coulombic orientational correlations in dilute aqueous electrolytes, J. Phys. Chem. Lett. **9**, 1985 (2018).

[38] P. Jungwirth and D. Laage, Ion-induced long-range orientational correlations in water: Strong or weak, physiologically relevant or unimportant, and unique to water or not? J. Phys. Chem. Lett. **9**, 2056 (2018).

[39] D. Borgis, L. Belloni, and M. Levesque, What does second-harmonic scattering measure in diluted electrolytes? J. Phys. Chem. Lett. **9**, 3698 (2018).

[40] J. Duboisset and P.-F. Brevet, Salt-induced long-to-short range orientational transition in water, Phys. Rev. Lett. **120**, 263001 (2018).

[41] J. Duboisset, F. Rondepierre, and P.-F. Brevet, Long-range orientational organization of dipolar and steric liquids, J. Phys. Chem. Lett. **11**, 9869 (2020).

[42] A. Chandra and B. Bagchi, The role of translational diffusion in the polarization relaxation in dense polar liquids, Chem. Phys. Lett. **151**, 47 (1988).

[43] B. Bagchi and A. Chandra, Polarization relaxation, dielectric dispersion, and solvation dynamics in dense dipolar liquid, J. Chem. Phys. **90**, 7338 (1989).

[44] G. Vijayadamodar, A. Chandra, and B. Bagchi, Effects of translational diffusion on dielectric friction in a dipolar liquid, Chem. Phys. Lett. **161**, 413 (1989).

[45] A. Chandra and B. Bagchi, Relationship between microscopic and macroscopic orientational relaxation times in polar liquids, J. Phys. Chem. **94**, 3152 (1990).

[46] S. Varghese, P. Illien, and B. Rotenberg, Dynamic correlations in a polar fluid: Confronting stochastic density functional theory to simulations, J. Chem. Phys. **163**, 124107 (2025).

[47] D. S. Dean and H. Diamant, Dielectric response as a source of viscosity in polar liquids, arXiv:2604.00262.

[48] C. Schröder, M. Haberler, and O. Steinhauser, On the computation and contribution of conductivity in molecular ionic liquids, J. Chem. Phys. **128**, 134501 (2008).

[49] D. Roy, N. Patel, S. Conte, and M. Maroncelli, Dynamics in an idealized ionic liquid model, J. Phys. Chem. B **114**, 8410 (2010).

[50] M. Sega, S. S. Kantorovich, A. Arnold, and C. Holm, in *Recent Advances in Broadband Dielectric Spectroscopy*, edited by Y. P. Kalmykov (Springer, Dordrecht, 2013), pp. 103–122.

[51] M. Sega, S. S. Kantorovich, C. Holm, and A. Arnold, Communication: Kinetic and pairing contributions in the dielectric spectra of electrolyte solutions, J. Chem. Phys. **140**, 211101 (2014).

[52] T. Hoang Ngoc Minh, J. Kim, G. Pireddu, I. Chubak, S. Nair, and B. Rotenberg, Electrical noise in electrolytes: A theoretical perspective, Faraday Discuss. **246**, 198 (2023).

[53] G. Pireddu, C. J. Fairchild, S. P. Niblett, S. J. Cox, and B. Rotenberg, Impedance of nanocapacitors from molecular simulations to understand the dynamics of confined electrolytes, Proc. Natl. Acad. Sci. USA **121**, e2318157121 (2024).

[54] M. R. Becker, R. R. Netz, P. Loche, D. J. Bonthuis, D. Mouhanna, and H. Berthoumieux, Dielectric properties of aqueous electrolytes at the nanoscale, Phys. Rev. Lett. **134**, 158001 (2025).

[55] P. Illien, A. Carof, and B. Rotenberg, Stochastic density functional theory for ions in a polar solvent, Phys. Rev. Lett. **133**, 268002 (2024).

[56] Note that τ_S is the *longitudinal* relaxation time of the polarization field. Within our description and approximations, the *transverse* relaxation time is simply given by $1/(D_S q^2 + 2D_S^r)$ [46,55].

[57] H. J. Bakker and J. L. Skinner, Vibrational spectroscopy as a probe of structure and dynamics in liquid water, Chem. Rev. **110**, 1498 (2010).

[58] D. Laage, G. Stirnemann, F. Sterpone, R. Rey, and J. T. Hynes, Reorientation and allied dynamics in water and aqueous solutions, Annu. Rev. Phys. Chem. **62**, 395 (2011).

[59] A. P. Thompson, H. M. Aktulga, R. Berger, D. S. Bolintineanu, W. M. Brown, P. S. Crozier, P. J. in 't Veld, A. Kohlmeyer, S. G. Moore, T. D. Nguyen, R. Shan, M. J. Stevens, J. Tranchida, C. Trott, and S. J. Plimpton, LAMMPS - a flexible simulation tool for particle-based materials modeling at the atomic, meso, and continuum scales, Comput. Phys. Commun. **271**, 108171 (2022).

[60] N. C. Maity, S. Mitra, and R. Biswas, Microscopic factors that dictate the optimal compositions of mixed solvent systems for lithium ion battery applications: Revelation through a combined experimental and simulation study, J. Phys. Chem. B **130**, 6920 (2026).

[61] M. Nakamoto, K. Endo, S. Katayama, J. Han, E. Otani, H. Watanabe, I. Okae, and Y. Umebayashi, Dielectric behavior of propylene carbonate solutions with LiPF6, LiClO4, and LiBF4. II. Molecular dynamics simulation study, J. Chem. Phys. **163**, 204504 (2025).

[62] M. Sha, X. Ma, N. Li, F. Luo, G. Zhu, and M. D. Fayer, Dynamical properties of a room temperature ionic liquid: Using molecular dynamics simulations to implement a dynamic ion cage model, J. Chem. Phys. **151**, 154502 (2019).

[63] S. Varghese, B. Rotenberg, and P. Illien, Data related to the article "Solvent-induced memory effects in a model electrolyte" [Data set], Zenodo, 2026, https://doi.org/10.5281/zenodo.23319414.

[64] M. Doi and S. F. Edwards, *The Theory of Polymer Dynamics* (Oxford University Press, Oxford, 1988).

[65] J. K. G. Dhont, *An Introduction to Dynamics of Colloids* (Elsevier, Amsterdam, 1996).

[66] S. Delong, F. Balboa Usabiaga, and A. Donev, Brownian dynamics of confined rigid bodies, J. Chem. Phys. **143**, 144107 (2015).

[67] I. M. Ilie, W. J. Briels, and W. K. den Otter, An elementary singularity-free rotational Brownian dynamics algorithm for anisotropic particles, J. Chem. Phys. **142**, 114103 (2015).

[68] R. Ramirez, R. Gebauer, M. Mareschal, and D. Borgis, Density functional theory of solvation in a polar solvent: Extracting the functional from homogeneous solvent simulations, Phys. Rev. E **66**, 031206 (2002).

[69] A. Toukmaji, C. Sagui, J. Board, and T. Darden, Efficient particle-mesh Ewald based approach to fixed and induced dipolar interactions, J. Chem. Phys. **113**, 10913 (2000).

[70] J. Zwanikken and R. van Roij, Inflation of the screening length induced by Bjerrum pairs, J. Phys.: Condens. Matter **21**, 424102 (2009).

[71] R. M. Adar, T. Markovich, and D. Andelman, Bjerrum pairs in ionic solutions: A Poisson-Boltzmann approach, J. Chem. Phys. **146**, 194904 (2017).